International Journal of Innovative
Computing, Information and Control
Volume 8, Number 4, April 2012
 ISSN 1349-4198
pp. 2777–2788

USING A LOW PASS FILTER TO RECOVER THREE-DIMENSIONAL SHAPE FROM FOCUS IN THE PRESENCE OF NOISE

Mannan Saeed Muhammad, Husna Mutahira and Tae-Sun Choi

Signal and Image Processing Lab
School of Mechatronics
Gwangju Institute of Science and Technology
No. 261, Cheomdan-gwagiro (Oryong-dong), Gwangju 500-712, Korea
{ mannan; husna; tschoi }@gist.ac.kr

Received November 2010; revised March 2011

Abstract. *Several passive methods like Shape from Focus (SFF) have been proposed for recovering 3-D shape of the objects from their 2-D images. Presence of noise in the images affects the accuracy of shape recovery. Most of the existing approaches show feeble performance when noise is present in the images. In this paper, we propose a new method based on a simple low pass filter, especially designed for SFF methods. The proposed scheme is experimented and evaluated using different image sequences of synthetic and real objects. It provides better results as compared with previous approaches; especially its performance is impressive for noisy images.*
Keywords: 3D shape reconstruction, Shape-from-focus, Depth estimation, Robustness, Focus measure, Noise

1. **Introduction.** Recovery of 3D shape from its 2D image can be broadly categorized into active and passive techniques. In active methods, sonar, laser range finders, etc. are included. Whereas, passive methods include shape from shading, shape from motion (motion parallax), stereo vision, shape from defocus and shape from focus. In microscopy active methods, being expensive, are sometimes impractical to use. Whereas, passive methods are more popular because of being cheap and easy to implement. Shape from focus (SFF) has many advantages over other passive methods such as stereo and motion parallax since these methods encounter the correspondence problem. However, accuracy of SFF methods needs to be further improved for better 3D shape.

In SFF methods, a stack of images is acquired by a single camera at different focus levels. The first step is to compute the focus quality of each pixel of every frame by applying a focus measure operator, and then the depth map is computed by maximizing focus value along the optical axis. A focus measure is defined as a quantity for locally evaluating the sharpness of a pixel. In literature, many focus measures have been reported in spatial as well as in transform domains. Laplacian, modified Laplacian, sum of modified Laplacian (SML), Tenenbaum, gray level variance (GLV) and M_2 are the famous focus measures among them [1, 2]. The Laplacian operator, being a point and symmetric operator, is a commonly used focus measure [3, 4, 5]. The focus value of an image is obtained by adding second derivatives in the x- and y-directions. In the case of textured images, the x and y components of the Laplacian operator may cancel out and subsequently yield no response [1]. Therefore, Laplacian is modified (ML), which can be computed by adding the squared second derivatives. Tenenbaum focus measure is based on first derivatives of and image in x- and y-directions. It is a gradient magnitude maximization method that measures the sum of the squared responses of the horizontal and vertical Sobel masks. For robustness,

it is also summed in a local window. One of the other well known focus measures is the GLV focus measure, based on the idea that in the case of a sharp image, the variance of the intensities is higher than that for a blurred image. The M_2 focus measure is actually modified version of Tenenbaum focus measure. The effects of illumination and change in window size on focus measure application in SFF have also been studied [6].

SFF can be implemented through a variety of techniques including traditional methods [4, 7, 8], wavelet analysis [9], neural networks [10], dynamic programming [3, 11], discrete cosine transform (DCT) [12], etc., but all these techniques start with the estimation of depth map using focus measures. Hence, the techniques for the estimation of this initial depth map become quite significant, and any error that occurred in them is carried forward to next stage, too. Also these algorithms must show robustness when the images used for SFF are corrupted with noise.

In this paper, we have proposed a new focus measure which normalizes the pixel values along the optical axis, and a Low-Pass-Filter is designed to remove the noise which consists of high frequencies. Then, the best focus points are found by maximizing the focus curve and the corresponding frame number is taken as depth for the particular point. The process is repeated to recover the shape of the object.

The paper is organized in the following way. In Section 2, some details of related work about SFF are given from the literature. Section 2.1 provides the motivation of the work. Section 2.2 describes the low pass filter. In Section 3, the proposed algorithm has been discussed. Section 4 gives the details of experimental setup. Section 5 describes the noise and its affects. Section 6 gives the results of shape reconstruction in the presence of noise and the comparisons with other commonly used focus measures. In Section 7, we have concluded the outcome of the results.

2. **Shape from Focus.**

In shape from focus (SFF) methods, a sequence of images are used, taken by a single camera at different focus levels, to compute the depth of the object in the scene. Focus measure (FM) operators are applied to this image sequence. Then, the entire image sequence is searched to find the best focused points in the image space; and, camera parameter settings are used to compute the distance of focused points. In Figure 1, the point 'P' is best focused at image distance 'Δ_i' from the lens. To compute the distance 'Δ_o' of the corresponding object-point, Thin-Lens-Formula is used:

$$\frac{1}{f} = \frac{1}{\Delta_i} + \frac{1}{\Delta_o}, \tag{1}$$

where 'f' is the focal length of the lens and 'Δ_o' is the object distance from the lens. The equation for the blur radius 'R' caused by the focusing of the object surface is given by Equation (2):

$$R = \frac{sD}{2}\left(\frac{1}{f} - \frac{1}{\Delta_i} - \frac{1}{\Delta_o}\right), \tag{2}$$

where 'D' is the diameter for the lens aperture and 's' is the distance for the image sensor plane from the lens as shown from Figure 1. Using Equation (1), when the point 'P' on the object is best focused in the focused plane, its corresponding pixel intensity value in the image is its true value (i.e., in a gray scale image, for white points on the body the pixel intensity value in the image will be near to maximum and for the black points the pixel intensity value will be near to minimum), whereas, when the point is defocused it will have the defused value (i.e., between white and black). This change in pixel intensity follows a 'Generalized Gaussian' curve [3]. Figure 2 shows the typical pixel behavior for two different pixels of an object in the image sequence.

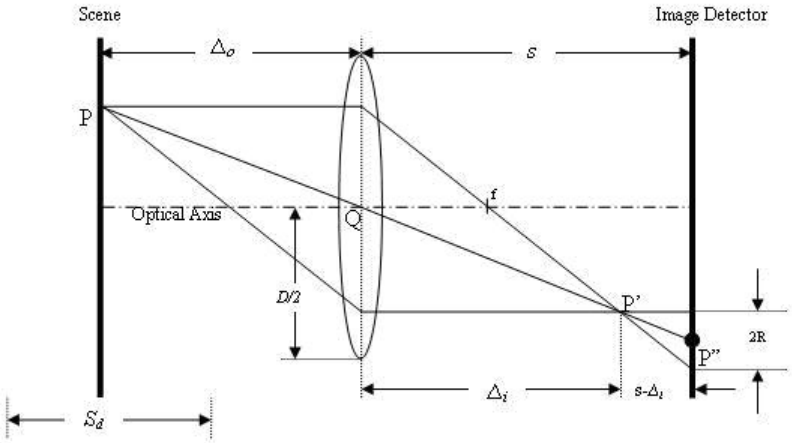

FIGURE 1. Camera system for SFF

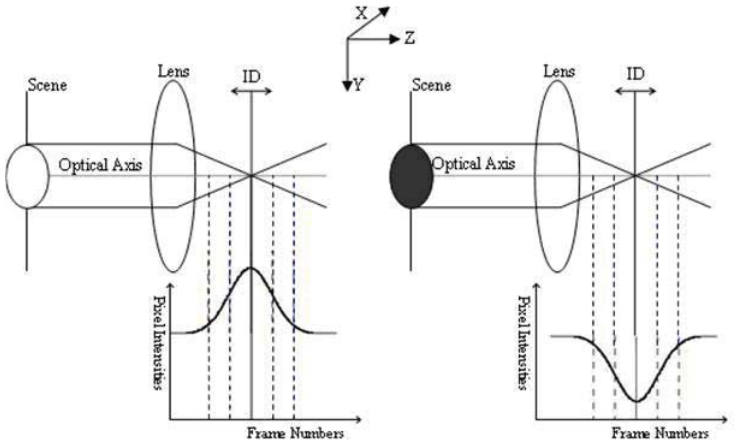

FIGURE 2. Pixel behavior in an image sequence ((left) white pixel and (right) black pixel)

2.1. **Motivation.** In conventional SFF methods, depth values for each object point are found by maximizing focus values, which are computed by using focus measures, along the optimal axis. Most of the focus measures reported in literature are either gradient based or statistical based focus measures. The gradient based focus measures, like Tenenbaum and SML, take the first and second derivatives of the image to compute the sharpness in the image. The statistical based focus measures, like GLV and normalize variance, exploit the statistical components of the image to find the focused regions in the image. In all these approaches, if a pixel is vitiated by noise, it affects the neighboring pixels too; for example if 3×3 window size is used then the corrupted pixel affects 24 other pixels in its neighborhood. In literature, the use of larger window size is employed to overcome this problem. However, taking a larger window size introduces averaging effect [1], and false depth detection occurs.

This phenomenon motivated us to propose a new method. As discussed in earlier, in the gray scale image, white object points are well focused at maximum gray levels, whereas, black object points are well focused at minimum gray levels. The suggested focus measure takes the values of a pixel along the optical axis in a single vector. Then, this vector is modified by subtracting the mean of the first and last values of the vector and taking the

square of the resultant. This helps us to reduce the two problems of finding maxima or minima of focus curve into a single problem of finding maxima only. A simple low pass filter (LPF) is designed to reduce the noise. The LPF is applied on these modified pixel values along the optical axis. Next section introduces the derivation of LPF.

2.2. **Low pass filter.** A low pass filter (LPF) is a filter that passes low frequency signals but attenuates signals with frequencies higher than the cutoff frequency. The combination of resistance and capacitance gives the time constant of the filter $\tau = RC$. The break frequency, also called the turnover frequency or cutoff frequency (in hertz), is determined by the time constant:

$$f_c = \frac{1}{2\pi\tau} = \frac{1}{2\pi RC}. \tag{3}$$

The effect of a LPF can be simulated on a computer by analyzing its behavior in the time domain, and then discretizing the model. According to Kirchoff's Laws and the definition of capacitance:

$$V_{out}(t) = V_{in}(t) - RC\frac{dV_{out}}{dt}. \tag{4}$$

This equation can be discretized. For simplicity, assume that samples of the input and output are taken at evenly spaced points in time separated by Δ_T time. Let the samples of V_{in} be represented by the sequence $(x_1, x_2, \ldots, x_n)$ and let V_{out} be represented by the sequence $(y_1, y_2, \ldots, y_n)$ which correspond to the same points in time. Making these substitutions:

$$y_i = x_i - RC\frac{y_i - y_{i-1}}{\Delta_T}, \tag{5}$$

and rearranging terms gives the recurrence relation:

$$y_i = x_i\frac{\Delta_T}{RC + \Delta_T} + y_{i-1}\frac{RC}{RC + \Delta_T}. \tag{6}$$

This discrete time implementation of a simple RC low pass filter is same as the '*exponentially weighted moving average*'.

3. **Proposed Algorithm.** In Figure 2, the vertical axis shows the 'pixel intensity' in gray scale image and horizontal axis shows 'image frame numbers' in the image sequence. From these figures it is clear that both 'white' and 'black' pixels in the image sequence have relatively very close values in defocused region, and only for focused regions these values vary from each other with great difference.

We modified these values according to the following:

$$\left[{}^{(i,j)}m_k\right]_{n\times 1} = \left[\sum_{\Omega,i',j'}\left({}^{(i+i',j+j')}p_k - \frac{\left[{}^{(i,j)}p_1 + {}^{(i,j)}p_n\right]}{2}\right)^2\right]_{n\times 1} \tag{7}$$

for all $1 \le k \le n$, where ${}^{(i,j)}p_k$ is the kth value in the original pixel intensity vector ${}^{(i,j)}P$; ${}^{(i,j)}p_1$ and ${}^{(i,j)}p_n$ are 1st and last values in pixel intensity vector; ${}^{(i,j)}m_k$ is the kth value in the modified pixel intensity vector ${}^{(i,j)}M$, i and j are the x and y position of the pixel in special domain, Ω is the summing window for the focus measure and n is the total number of images in the image sequence, given by Equation (8):

$$n = \frac{S}{\Delta_{step}}, \tag{8}$$

where S is the total displacement of object plane and Δ_{step} is the step size.

LPF is then applied to the modified pixel intensity vector to remove the noise. Equation (9) yields the final focus curve of the proposed focus measure.

$$^{(i,j)}y_k =^{(i,j)} m_k \left(\frac{1}{\sigma_1\sigma_2+1}\right) +^{(i,j)} y_{k-1}\left(\frac{\sigma_1\sigma_2}{\sigma_1\sigma_2+1}\right), \tag{9}$$

where σ_1 and σ_2 are tuned for the LPF. The lag in the focus curve is given by $l = \sigma_1\sigma_2$. The depth map of the data point (i, j) is recovered by the following:

$$^{(i,j)}D = \left[\arg\max_k \left(^{(i,j)}y_k\right)\right] - l \tag{10}$$

where $1 \leq k \leq n$.

4. **Experimental Setup.** For experiments we have used five different objects (simulated cone, real cone, real plane, coin and LCD-filter). The simulated cone images are generated by computer simulations. The real cone and real plane are made from hardboard with black and white stripes drawn on the surface so that a dense texture is observed in the images when taken from the CCD camera system. The details of simulated cone, real cone and real plane are given in [13], we have used the same image sequences. The coin images are the magnified images on Lincoln's head at the back of (US) one-cent coin. The LCD images are microscopic images of LCD-TFT display.

All the images are taken by varying the object plane by 'Δ_{step}', and are stored in a sequence on every step such that: (i) the object moves towards (or away from) the lens assuring that the complete object is first defocused then gradually it focuses (on every point) and then it is again completely defocused; (ii) there is no change in magnification when the images are taken [3].

Figure 3 shows frames 1st to last of the simulated cone. The images show that the simulated cone follows the above statements (1&2). Figure 4 shows the 10th image in the image stack for real cone, real plane, coin and LCD-TFT.

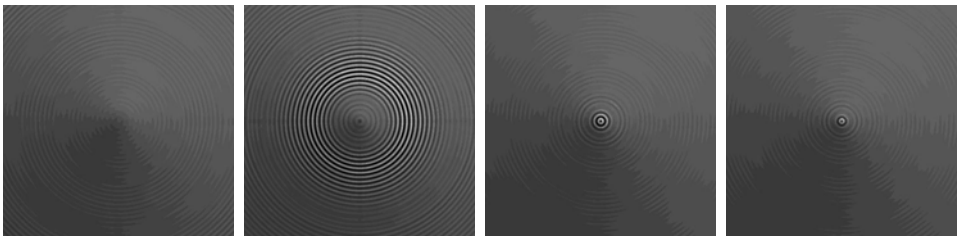

(a) First (b) 50th (c) 90th (d) Last

FIGURE 3. Image frames of simulated cone image sequence

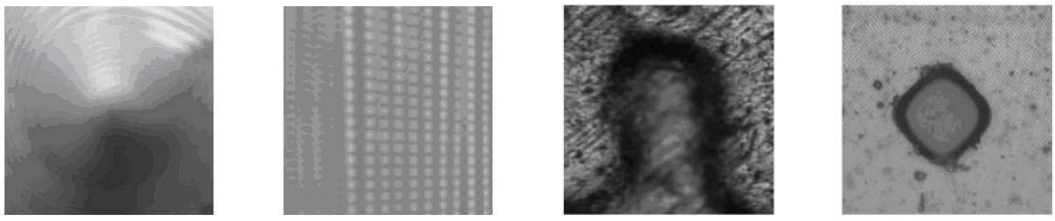

(a) Real cone (b) Real plane (c) Coin (d) LCD-TFT

FIGURE 4. 10th image frame of each image sequence

(a) Gaussian (b) Shot (c) Speckle

FIGURE 5. Frame 10th of simulated cone corrupted with different noise with $\mu = 0$ and $\sigma = 0.005$

5. **Effects of Noise on Shape Reconstruction.** When the images used for SFF are corrupted with noise, the computation of depth map becomes difficult. In real time applications, various type of noises (like Rayleigh, Exponential, Uniform, Shot, Speckle and Gaussian) may occur. Therefore, a robust method is required to deal with noisy situations.

Many focus measures discussed in the literature are based on the second-derivative on the image gradient and hence, are more prone to noise. Laplacian and its variants are based on second-derivative, whereas Tenenbaum is based on single derivative technique which is again sensitive to noise (but less than second-derivative techniques). Similar problems occur when mean and variances are incorporated as a focus measure.

We have used Gaussian noise, shot noise and speckle noise [12, 14, 15, 16], to the image sequence with zero mean ($\mu = 0$) and different variances, to compare our results. The results are compared and discussed in the next section. Figure 5 shows the 10th frame of the simulated cone image sequence, degraded by the Gaussian noise, shot (salt and pepper) noise and speckle noise.

6. Results and Discussion.

6.1. Metric measures.

An image quality metric can be defined as a measure of the perceived difference from a reference image. The fundamental assumption is that, any reduction in quality is caused by some perceived difference. In this paper, the image quality metrics are implemented to depth map comparison. If no differences can be perceived, then the computed depth map is indistinguishable from the original shape and the shape-quality is at its maximum. Hundreds of metrics have been proposed to deal with both general and specific aspects. Some of the metrics are mentioned here.

6.1.1. *Mean squared error and root mean squared error.* Mean squared error (MSE) [2, 9, 17, 18] is one of the many ways to quantify the amount by which depth maps differ from each other. MSE measures the average of square of the 'error'. It is the second moment (about the origin) of the error and is defined as follows:

$$MSE = \frac{1}{MN} \sum_{j=0}^{M-1} \sum_{i=0}^{N-1} |{}^{(i,j)}D_{org} - {}^{(i,j)}D|^2,$$

where M is the number of horizontal pixels in the image and N is the number of vertical pixels, ${}^{(i,j)}D_{org}$ is the original Depth map and ${}^{(i,j)}D$ is the computed depth map. Root mean squared error (RMSE) is simply the square-root of MSE; $RMSE = \sqrt{MSE}$.

6.1.2. *Peak signal-to-noise ratio.* The peak signal-to-noise ratio (PSNR) [2, 9, 17, 18] is the ratio between the maximum possible power of signal and the power of corrupting noise that affects the fidelity of its representation. Because many signals have wide dynamic range, PSNR is usually expressed in terms of logarithmic decibel scale (dB):

$$PSNR = -10 \log_{10} \left(\frac{MSE}{D_{\max}^2} \right),$$

where $D_{\max}$ is the maximum pixel value.

6.1.3. *Correlation.* Correlation or Correlation-Coefficient [19] is a metric measure that indicates the strength and direction of a linear relationship between two images. In general, correlation refers to the departure of two images from independence. The correlation coefficient is computed as:

$$Cor. = \frac{\sum_i \sum_j ({}^{(i,j)}D_{org} - \mu_{org})({}^{(i,j)}D - \mu_c)}{\sqrt{\sum_i \sum_j ({}^{(i,j)}D_{org} - \mu_{org})^2 \sum_i \sum_j ({}^{(i,j)}D - \mu_c)^2}}$$

where ${}^{(i,j)}D_{org}$ is the original depth map, μ_{org} is its mean, ${}^{(i,j)}D$ is the computed depth and μ_c is its mean.

We have used RMSE, correlation and PSNR given in above equations to compare the results.

6.2. **3D shape reconstruction results.** We used five different objects described earlier (simulated cone, real cone, real plane, coin and LCD) for the comparison, as shown in Figures 3 and 4. Figures 6(a) and 6(c) show the behavior of white and black pixels in the image sequence. Both type of pixels have nearly similar values (or have less difference) where they are defocused and differ a lot when focused. In Figures 6(b) and 6(d), the modified pixel behavior in an image sequence is shown for both white and black pixels along with the corresponding responce of LPF, respectively.

We chose SML, GLV, M_2 and Tenenbaum as they are the most commonly used FMs, to compare with our FM. We found out that the RMSE is lowest, whereas, correlation and PSNR is highest with proposed method. Table 1 shows the RMSE, correlation and PSNR for the shape reconstruction for simulated cone, compared with the traditional FMs (SML, GLV, M_2 and Tenenbaum). It is clear from Table 1, that the proposed method gives us better results than that of the traditional FMs. Table 1 also shows that the

TABLE 1. Metric measures for depth estimation methods by different FMs for simulated cone and real cone

EXPERIMENTED OBJECT	**FOCUS MEASURES**	**RMSE**	**COR.**	**PSNR**
Simulated Cone	SML	12.4475	0.7389	17.8823
	GLV	10.9586	0.8021	18.1438
	M_2	10.8687	0.8081	18.2154
	Tenenbaum	10.8675	0.8016	18.2153
	Proposed	**8.3706**	**0.9515**	**20.4837**
Real Cone	SML	15.4441	0.5824	15.1489
	GLV	10.21551	0.716	18.7048
	M_2	10.2363	0.7148	18.6868
	Tenenbaum	10.2886	0.7112	18.6425
	Proposed	**2.0427**	**0.9332**	**32.6868**

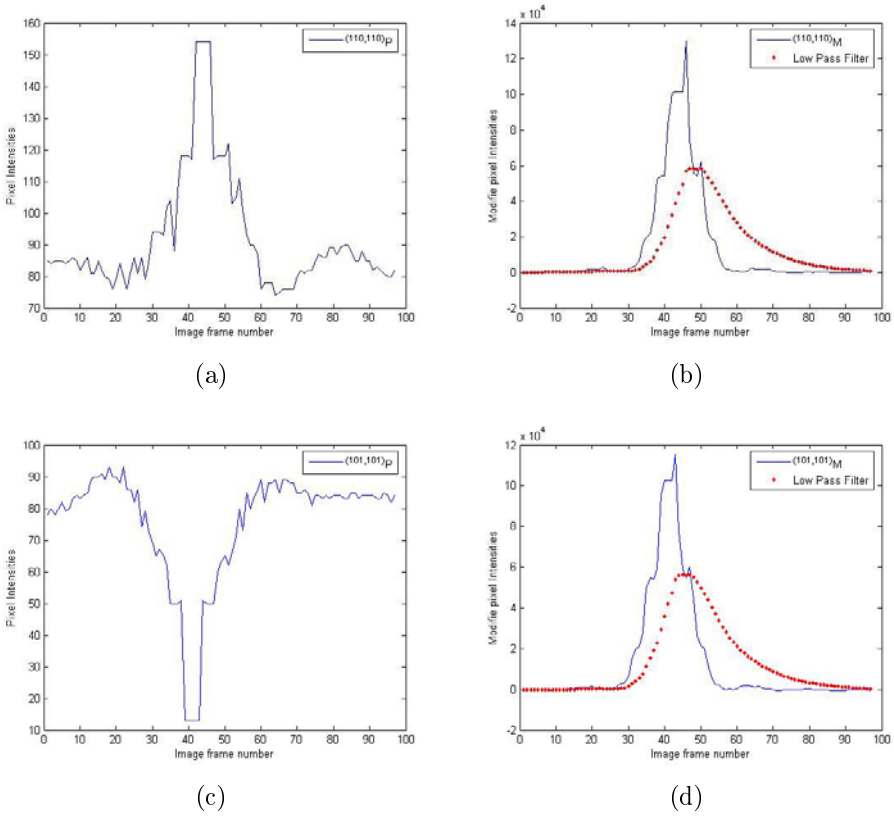

(a) (b)

(c) (d)

FIGURE 6. Examples of pixel behavior and modified pixel behavior in an image sequence for a simulated cone

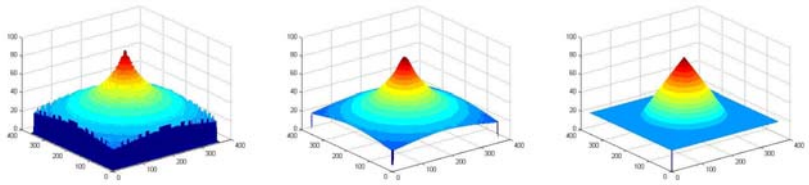

(a) (b) (c)

FIGURE 7. 3D representation of simulated cone, (a): by M_2, (b): by proposed FM and (c): original depth map of simulated cone

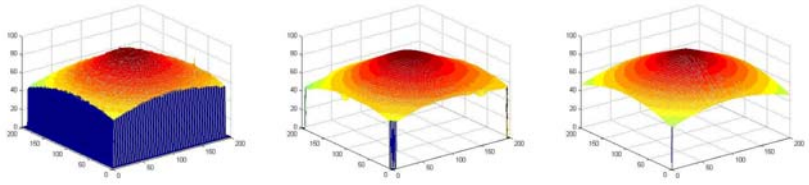

(a) (b) (c)

FIGURE 8. 3D representation of real cone, (a): by M_2, (b): by proposed FM and (c): original depth map of simulated cone

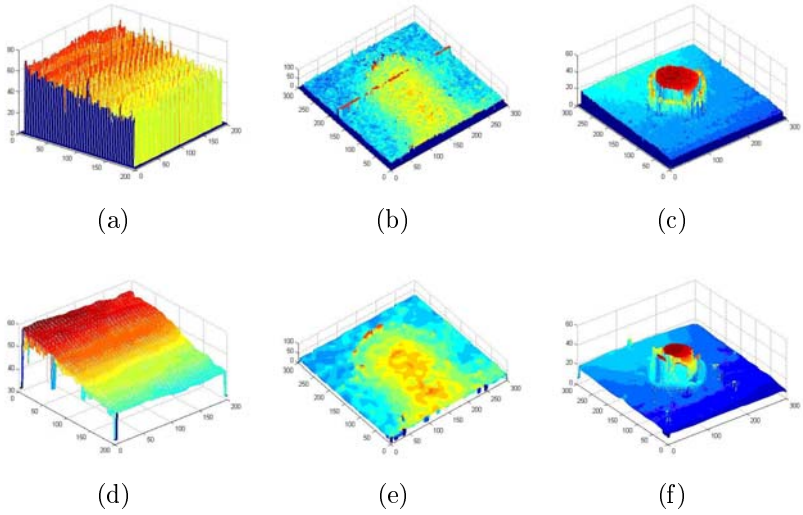

(a) (b) (c)

(d) (e) (f)

FIGURE 9. 3D representation M_2 (top row) and proposed method (bottom row) of ((a) and (d)) real plane, ((b) and (e)) coin and ((c) and (f)) LCD-TFT filter

TABLE 2. Metric measures for depth estimation methods by different FMs for simulated cone, with Gaussian, Shot and Speckle noises with $\mu = 0$ and $\sigma = 0.005$

NOISE TYPE	FOCUS MEASURES	RMSE	COR.	PSNR
Gaussian	SML	35.0583	0.0619	8.0430
	GLV	11.1016	0.8007	18.0312
	M_2	11.3369	0.7949	17.8490
	Tenenbaum	11.0811	0.8001	15.7781
	Proposed	**9.6961**	**0.9511**	**19.2070**
Shot	SML	11.4083	0.7860	17.7945
	GLV	11.2605	0.7928	17.9077
	M_2	22.6157	0.3987	11.8507
	Tenenbaum	11.0167	0.7994	18.0979
	Proposed	**8.5890**	**0.9506**	**20.2600**
Speckle	SML	15.6328	0.6309	15.0581
	GLV	11.1608	0.7984	17.9849
	M_2	11.2472	0.7996	17.9180
	Tenenbaum	11.1411	0.7963	18.0003
	Proposed	**9.7175**	**0.9512**	**19.1878**

proposed method has the highest correlation and PSNR, and lowest RMSE for the real cone. Figure 7 shows the reconstruction of simulated cone by M_2 compared with the proposed method. Figures 8 and 9 show the reconstruction of real cone, real plane, coin and LCD filter. It is clear from these figures that the 3D shape representation using the proposed method, when there is no noise, is much smoother than that of traditional FMs. The depth map obtained using the proposed method is clear, but the depth map with the traditional FMs has degraded significantly.

Table 2 shows the comparison of RMSE of different methods with the proposed method, when Gaussian noise ($\mu = 0$, $\sigma = 0.005$) is added to the image sequence. The tables show

TABLE 3. Metric measures for real cone for Gaussian noise ($\mu = 0$, $\sigma = 0.0005$)

FOCUS MEASURES	RMSE	COR.	PSNR
SML	14.1915	0.6402	15.8491
GLV	10.4969	06.991	18.4684
M2	11.7156	0.6293	17.5143
Tenenbaum	10.6057	0.6924	18.3789
Proposed	2.9429	0.8646	29.5141

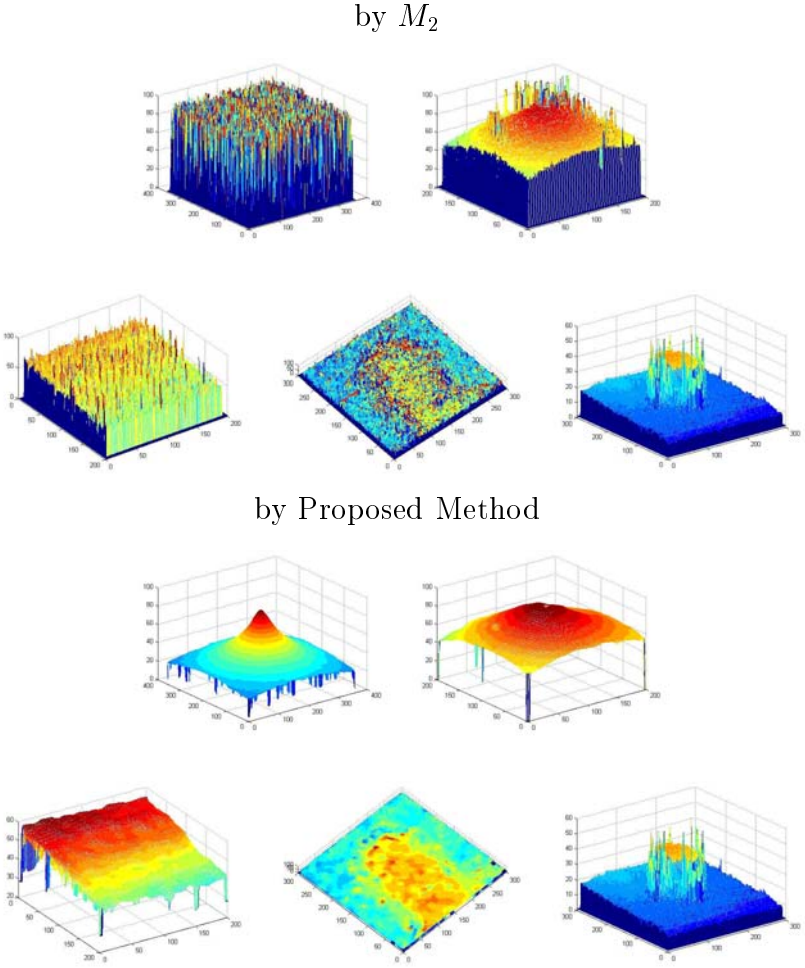

FIGURE 10. 3D representation of experimented objects in the presence of Gaussian noise $\mu = 0$ and $\sigma = 0.005$, left to right: simulated cone, real cone, real plane, coin and LCT-TFT

the proposed method not only works well for 'no noise' but also give good RMSE. Table 2 also shows that the comparison of correlation and also supports the same results. It is also clear from table that the correlation coefficient of the proposed method is the highest among all the focus measures. In the same table the comparison of PSNR is also given by different FMs with Gaussian noise ($\mu = 0$, $\sigma = 0.005$). The PSNR for the proposed method is also good among the other FMs. Figure 10 shows the reconstruction of simulated cone by different methods when Gaussian noise ($\mu = 0$, $\sigma = 0.005$) is added to the image sequence.

by M_2

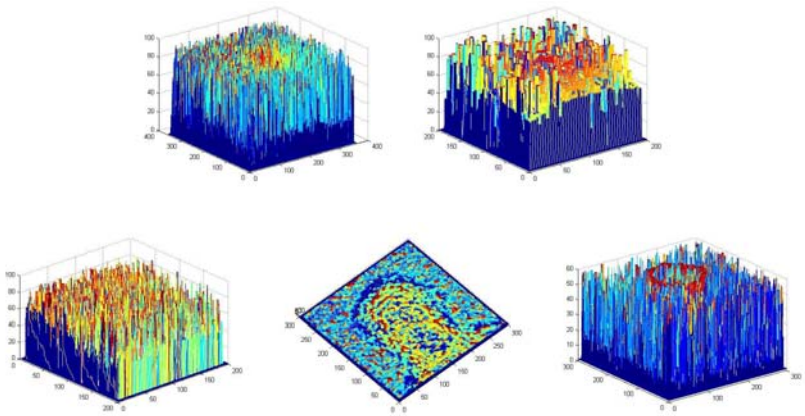

by Proposed Method

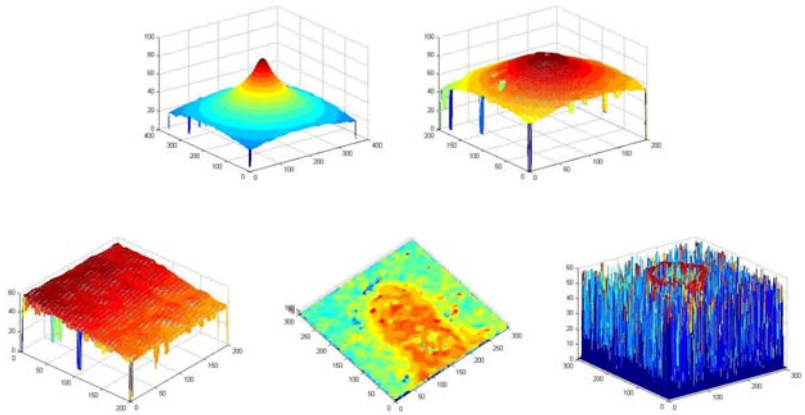

FIGURE 11. 3D representation of experimented objects in the presence of shot noise $\mu = 0$ and $\sigma = 0.005$, left to right: simulated cone, real cone, real plane, coin and LCT-TFT

Also, in Table 2, the RMSE, correlation and PSNR for simulated cone is provided, when used images are degraded by shot noise (with $\mu = 0$, $\sigma = 0.005$). The results clearly demonstrate that the proposed method has shown robustness against shot noise.

Figure 11 shows the reconstruction of simulated cone in the presence of shot noise ($\mu = 0$, $\sigma = 0.005$). The smooth surface is clearly visible in the figures.

In Table 3, the equivalent results are shown for the real cone. It is clear from Table 3 that the proposed method has minimum RMSE and highest correlation and PSNR values. In Figures 10 and 11, the shape reconstruction for the real plane, coin and LCD are given with the Gaussian and shot noise ($\mu = 0$, $\sigma = 0.005$), with M_2 used as a focus measure.

7. **Conclusions.** In this paper, we have proposed a new focus measure especially designed for the shape reconstruction using focus based passive method (Shape from Focus). For this purpose, we have developed a simple but robust algorithm to calculate best focused point using the idea of a simple RC Low Pass Filter. The proposed FM has shown good results even in the presence of noise.

In Shape from Focus the images are taken by varying the focus values in different steps, and each pixel in the image is taken as a single measurement. The thin-lens-model is used to estimate the change in pixel's energy. The pixel values are modified by subtracting the maximum of first and last frame along the optical axis. An analogous of a simple RC

filter is used to eliminate the noise present in the modified values. The maximum value in the modified pixel intensity vector and its corresponding frame number is searched. The proposed method is more precise as compared with previous methods and also the robustness of the method to accommodate different types of noise at different standard deviations makes the FM more vigorous against noisy measurements. The results are compared using RMSE, Correlation and PSNR.

Acknowledgment. This work was supported by the National Research Foundation of Korea Grant funded by the Korean Government (NRF-2010-013-D00068).

REFERENCES

[1] A. S. Malik and T. S. Choi, Consideration of illumination effects and optimization of window size for accurate calculation of depth map for 3D shape recovery, *Pattern Recognition*, vol.40, no.1, pp.154-170, 2007.

[2] A. M. Eskicioglu and P. S. Fisher, Image quality measures and their performance, *IEEE Trans. on Communications*, vol.43, no.12, pp.2959-2965, 1995.

[3] S. M. Mannan, A. S. Malik and T. S. Choi, A fast algorithm using pixel-intensities as a model for depth measurement, *IEEE International Conference on Consumer Electronics*, 2008.

[4] M. Noguchi and S. K. Nayar, Microscopic shape from focus using active illumination, *IEEE International Conference on Pattern Recognition*, pp.147-152, 1994.

[5] M. Asif and T. S. Choi, Shape from focus using multilayer feed-forward neural networks, *IEEE Transactions on Image Processing*, vol.10, no.11, 2001.

[6] F. S. Helmli and S. Scherer, Adaptive shape from focus with an error estimation in light microscopy, *The 2nd Int. Symposium on Image and Signal Processing and Analysis*, pp.188-193, 2001.

[7] M. B. Ahmad and T. S. Choi, A heuristic approach for finding best focused shape, *IEEE Transactions on Circuits and Systems for Video Technology*, vol.15, no.4, pp.566-574, 2005.

[8] M. B. Ahmed and T. S. Choi, Fast and accurate 3-D shape from focus using dynamic programming optimization technique, *IEEE International Conference on Acoustics, Speech and Signal Processing*, vol.2, 2005.

[9] G. Cassella and E. L. Lehmann, *Theory of Point Estimation*, Springer, 1999.

[10] J. Yun and T. S. Choi, Accurate 3-D shape recovery using curved window focus measure, *IEEE International Conference on Image Prrocessing*, vol.3, pp.910-914, 1999.

[11] M. Subbarao, T. S. Choi and A. Nikzad, Focusing techniques, *Optical Eng.*, vol.32, no.11, pp.2824-2836, 1993.

[12] M. T. Mahmood, A. Khan and T. S. Choi, Approximating 3D shape through Bezier curve and moments in discrete cosine transform, *International Journal of Innovative Computing, Information and Control*, vol.5, no.10(A), pp.2947-2957, 2009.

[13] M. Subbarao and T. S. Choi, Accurate recovery of three-dimensional shape from image focus, *IEEE Transactions on Pattern Analysis and Machine Intelligence*, vol.17, no.3, pp.266-274, 1995.

[14] A. Hussain, M. A. Jaffar and A. M. Mirza, Detail preseving fuzzy filter for impulse noise romaval, *International Journal of Innovative Computing, Information and Control*, vol.5, no.10(B), pp.3583-3591, 2009.

[15] A. Hussain, M. A. Jaffar and A. M. Mirza, Random-valued impulse noise removal using fuzzy logic, *International Journal of Innovative Computing, Information and Control*, vol.6, no.10, pp.4273-4288, 2010.

[16] A. Hussain, M. A. Jaffar, Z. Ul-Qayyum and A. M. Mirza, Directional weighted median based fuzzy filter for random valued impuse noise removal, *ICIC Express Letters, Part B: Applications*, vol.1, no.1, pp.9-14, 2010.

[17] A. C. Bovik, *Handbook of Image and Video Processing*, Elsevier, 2005.

[18] Z. Wang and A. C. Bovik, A universal image quality index, *IEEE Signal Processing Letters*, vol.9, no.3, pp.81-84, 2002.

[19] J. L. Rodgers and W. A. Nicewander, Thirteen ways to look at the correlation coefficient, *The American Statistician*, vol.42, pp.59-66, 1988.